CHEMISTRY
A European Journal

A Journal of
ChemPubSoc Europe

Accepted Article

Title: Cascade amplified time-resolved fluorescent assay driven by enzyme-integrated catalytic compartment as an artificial multi-enzyme complex

Authors: Jie Gao, Caihong Wang, Jinhong Wang, and Hongliang Tan

To be cited as: *Chem. Eur. J.* 10.1002/chem.201902222

Link to VoR: http://dx.doi.org/10.1002/chem.201902222

Supported by
ACES

WILEY-VCH

10.1002/chem.201902222

WILEY-VCH

COMMUNICATION

Cascade amplified time-resolved fluorescent assay driven by enzyme-integrated catalytic compartment as an artificial multi-enzyme complex

Jie Gao[#], Caihong Wang[#], Jinhong Wang, and Hongliang Tan* [a]

Abstract: We here report a simple and efficient strategy of fabricating artificial multi-enzyme complex (MEC) based on the integration of natural enzyme with catalytic compartment. As a proof of concept, this strategy was demonstrated by selecting cholesterol oxidase (ChOx) and Ce(III)-based nanoscale coordination polymer (Ce-NCP) with peroxidase-like activity as the models, which forms ChOx@Ce-NCP. Benefiting from the confinement and sheltering effects of Ce-NCP, superior cascade activity and stability in harsh environments were achieved in ChOx@Ce-NCP. Meanwhile, the distinct advantage of ChOx@Ce-NCP has also been highlighted by its negligible substrate inhibition effect and adjustable mass ratio of building blocks. Upon the doping of Tb(III) in ChOx@Ce-NCP, a luminescent artificial MEC (ChOx@Ce-NCP:Tb) was further fabricated to drive a cascade amplified time-resolved fluorescent assay within a confined space, showing high sensitivity and specificity toward cholesterol.

In biological system, multi-enzyme complex (MEC) is a highly ordered assembly of multiple enzymes and involves in a major class of chemical transformation for mediating signal transductions and metabolic pathways [1]. Unlike free-floating enzymes, MEC enables intermediates to be effectively transported between the active sites on enzyme subunits without leaving the MEC, resulting in a high local concentration of intermediates to promote overall catalytic efficiencies toward desired pathways [2]. Inspired by nature, significant efforts have been devoted to building artificial MEC [3]. The most common approach is to confine multiple natural enzymes together within a nanoscaled compartment [4]. Although encourage results have been achieved by such approach, the involvement of multiple natural enzymes also brings it several drawbacks. For example, to tolerate the various properties of different enzymes, an appropriate compartment has to be designed and prepared very carefully [5]. This makes the fabrication process of artificial MEC complicated and laborious. Moreover, as a trade-off of high loading efficiency, the overall turnover of artificial MEC is often limited by the substrate inhibition effect that caused by excess intermediates in the confined space. A typical example of such effect is the irreversible inactivation of horseradish peroxidase (HRP) at high local concentration of H_2O_2, which is often found in the artificial MEC coupled glucose oxidase with HRP [6].

As a fascinating artificial enzyme, nanozyme has been extensively investigated in a variety of fields due to its unique catalytic features [7]. Particularly, tremendous interests have recently been aroused in the fabrication of hybrid catalyst by coupling nanozyme with natural enzyme [8]. This is because such hybrid catalyst endows nanozyme with the ability to specially recognize substrates while eliminating the substrate inhibition effect of natural enzyme. Within this point, the hybrid catalyst might be an ideal artificial MEC for driving cascade reactions. However, the cascade reactions catalyzed by such hybrid catalyst were mostly performed in a bulk solution but not a confined space, and thereby only a low overturn was obtained due to the diffusion losses of intermediates during transportation. Additionally, the fabrications of the hybrid catalysts are often complicated and low efficiency as the requirement of covalent binding between natural enzyme and nanozyme [9]. A solution to the issues may be offered by co-encapsulating natural enzyme and nanozyme into one compartment. However, the mass ratios of these two catalysts are technically difficult to be precisely controlled as natural MEC in the process of encapsulation.

Herein, we present a new strategy to fabricate artificial MEC by integrating natural enzyme with catalytic compartment. Different from conventional compartments that used only for enzyme encapsulation, the catalytic compartment plays two roles of host and catalyst, which act synergistically to drive cascade reactions. As a host, the compartment offers a confined space to allow effective transportation of intermediates with minimized diffusion losses while protecting loaded enzymes against harsh environments. When it performed as a catalyst, the compartment involves in the cascade reaction and eliminates the substrate inhibition effect to ensure product generation with high efficiency. In addition, the artificial MEC is essentially a hybrid catalyst of natural enzyme and nanozyme and its formation only involves in the encapsulation of single enzyme, and thereby a high encapsulation efficiency and adjustable mass ratio of the cascade catalysts are expected as natural MEC.

To demonstrate this strategy, nanoscale coordination polymer (NCP) may be an ideal candidate of catalytic compartments due to its well demonstrated advantages in hosting and mimicking natural enzymes as compared to conventional hosts and nanozymes [10]. Nevertheless, to our knowledge, the role of NCP has been only limited to either a stabilizing host scaffold or an enzyme mimic till now, whereas the investigations on combining these two merits into one composite for driving cascade reaction remain unexplored.

As a proof of the concept, Ce(III)-based NCP (Ce-NCP) with peroxidase-like activity was selected as a model to integrate cholesterol oxidase (ChOx) for fabricating the artificial MEC, denonted as ChOx@Ce-NCP. Adenosine triphosphate (ATP) was used as a bridge linker to synthesize the Ce-NCP because of its good water solubility and biocompatibility. **Figure S1** shows that the Ce-NCP is spheroid with diameter ranging from 10 to 30 nm and its formation is originated from the chemical coordination of Ce^{3+} with the phosphate and nucleobase moieties of ATP [11]. The

[a] Jie Gao, Caihong Wang, Jinhong Wang, and Hongliang Tan
Key Laboratory of Chemical Biology of Jiangxi Province
College of Chemistry and Chemical Engineering
Jiangxi Normal University
Nanchang, 330022, China
E-mail: hltan@jxnu.edu.cn

[#] Jie Gao and Caihong Wang contributed equally to this work.

Supporting information for this article is given via a link at the end of the document.

10.1002/chem.201902222

powder XRD pattern reveals that the Ce-NCP is structurally amorphous (**Fig. S2a**). From the N_2 isotherm in **Fig. S2b**, we can see that the Ce-NCP has a BET surface area of 486.37 m^2 g^{-1} and an average pore size of 2.16 nm, indicating its porosity nature. The peroxidase-like activity of Ce-NCP was demonstrated by typical TMB colorimetric assay (**Fig. S3**) and its highest activity was found at pH 6.0 (**Fig. S4**). Based on the fluorescent assay of terephthalic acid and electron spin resonance spectrum (**Fig. S5**), the catalytic mechanism of the Ce-NCP can be ascribed to its Fenton behavior in decomposing H_2O_2 to $^{\bullet}OH$ [12]. By further investigating steady-state kinetics (**Fig. S6** and **Table S1**), it was found that compared with HRP, the Ce-NCP has a higher affinity and a faster reaction rate to the substrates (H_2O_2 and TMB), demonstrating its excellent catalytic performances.

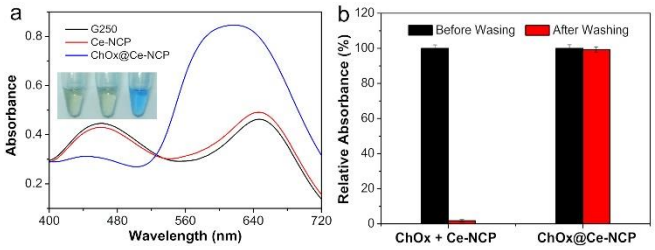

Figure 1. (a) Colorimetric assay of coomassie brilliant blue G-250 with Ce-NCP and ChOx@Ce-NCP. (b) Relative absorbance of coomassie brilliant blue G-250 in the presence of SDS-treated ChOx@Ce-NCP and the mixture of ChOx and Ce-NCP.

The self-assembly of Ce^{3+}, ATP and ChOx leads to the formation of ChOx@Ce-NCP. By staining with coomassie brilliant blue G-250 (**Fig. 1a**), we can see that ChOx@Ce-NCP exhibits a bright blue with the maximum absorbance at 595 nm, whereas the absorption spectrum and color of Ce-NCP are the same as that of the dye control. This suggests that ChOx has been presented, which is confirmed by the observation of characteristic amide I band (1645 cm^{-1}) and II band (1510 cm^{-1}) of protein in FTIR spectrum (**Fig. S7**). On this basis, the immobilization mode of ChOx in Ce-NCP was investigated by treating ChOx@Ce-NCP with excess sodium dodecylsulfate (SDS). Under this condition, any surface-absorbed proteins will be removed. However, we found from **Fig. 1b** that after washing thoroughly, the protein colorimetric assay was not affected by the SDS treatment, demonstrating that ChOx was indeed entrapped inside the Ce-NCP rather than adsorbed on its surface. With the calibration curve in **Fig. S8**, the encapsulation efficiency of ChOx in Ce-NCP was determined as 79.1 %, which is much higher than that of conventional hosts such as porous silica (15 %) [13]. Nevertheless, the ChOx@Ce-NCP still remained the same morphology (**Fig. S9**) and structure (**Fig. S10**) as pure Ce-NCP, suggesting that the structure of Ce-NCP is free from ChOx. This is verified by the negligible changes of ChOx@Ce-NCP in the average hydrodynamic diameter (**Fig. S11**). The unchanged structure of ChOx@Ce-NCP can be attributed to the adaptive inclusion property of Ce-NCP as a compartment, which follows the shape of ChOx to flexibly rearrange its structures during self-assembly processes [10a].

Since ChOx can catalyze cholesterol (Chol) to produce H_2O_2, a cascade reaction might be initiated by Chol with the formation of ChOx@Ce-NCP. To confirm this speculation, the absorption spectra of TMB solutions with Chol were measured at different conditions. As depicted in **Fig. 2a**, only the addition of ChOx@Ce-NCP can cause a typical oxTMB absorption spectrum, while almost no oxTMB absorbance was recorded in the presence of individual ChOx or Ce-NCP. This indicates that TMB oxidation is accomplished by combining the activities of ChOx and Ce-NCP, which leads to a cascade reaction. Specifically, this cascade reaction begins with the conversion of Chol by ChOx to cholest-4-en-3-one and H_2O_2, and followed by the oxidation of TMB by Ce-NCP to generate oxTMB with the assistant of the produced H_2O_2 (**Fig. 2b**). On the other hand, the occurrence of this cascade reaction also reflects that Ce-NCP as a compartment is permeable to Chol. This is further demonstrated by the enhanced oxTMB absorbance at high concentration of Chol (**Fig. S12**). Taken together, ChOx@Ce-NCP has been successfully fabricated and it is capable of driving one-pot cascade reaction.

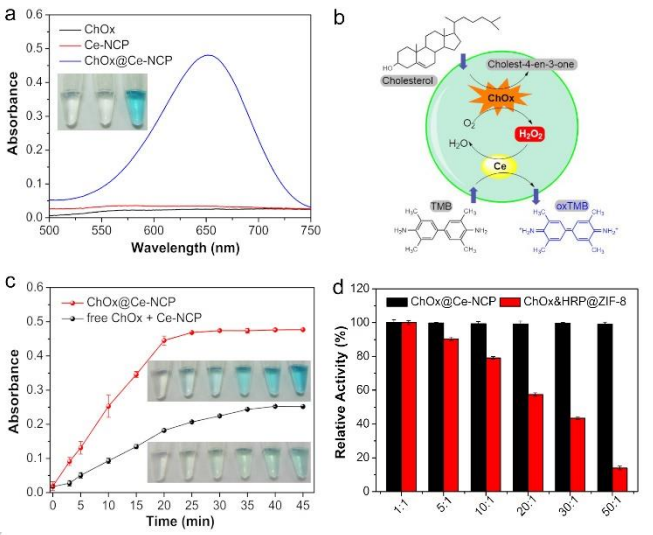

Figure 2. (a) Absorption spectra and photography of TMB solutions with ChOx, Ce-NCP and ChOx@Ce-NCP after adding Chol. (b) Schematic illustration of Chol-triggered TMB oxidation by ChOx@Ce-NCP. (c) Time-dependent absorbance and color changes of oxTMB catalyzed by ChOx@Ce-NCP and the mixture system of free ChOx and Ce-NCP. (d) Relative activity of ChOx@Ce-NCP and ChOx&HRP@ZIF-8 with molar ratios of ChOx to Ce-NCP (or HRP) from 1:1 to 50:1.

The catalytic performances of ChOx@Ce-NCP were then evaluated by monioring oxTMB absorbance at different intervals. **Fig. 2c** shows that upon reaction time increasing, ChOx@Ce-NCP can lead to an intensified oxTMB absorbance, which is same as that of the mixture system of free ChOx and Ce-NCP. The same trends indicate that these two cascade systems share a same catalytic pathway. However, ChOx@Ce-NCP brings a higher oxTMB absorbance at all stages, and an obvious 3-min lag phase of oxTMB absorbance increase was found in the mixture system. This reflects that ChOx@Ce-NCP can induce a faster TMB conversion, which is consistent with its higher catalytic activity (**Fig. S13**). Since identical reaction conditions are used in these two cascade systems, the superior activity of ChOx@Ce-NCP is attributed to the close proximity of ChOx to Ce-NCP within a confined space. In this case, the intermediate H_2O_2 is able to be

generated in site and presented with a high local concentration in the confined space of Ce-NCP. As a result, the produced H_2O_2 will be allowed to effectively transfer from ChOx to Ce-NCP without leaving the confined space, which minimizes the diffusion losses of H_2O_2 during transportation, and consequently leading to an enhanced cascade activity in the ChOx@Ce-NCP.

Because high local concentration of intermediates can often cause a substrate inhibition effect to give a low cascade activity in the co-encapsulated cascade systems, the effect of H_2O_2 on ChOx@Ce-NCP was investigated. To this end, we conducted a series of Chol conversion experiments that catalyzed by ChOx@Ce-NCP with different molar ratios of ChOx and Ce-NCP, as local H_2O_2 concentrations were determined by ChOx amounts [6a]. From **Fig. 2d**, it can be seen that upon the increase of ChOx amounts, the TMB oxidation reactions almost no suppressed, suggesting that high local concentration of H_2O_2 has a negligible inhibition effect to the cascade activity of ChOx@Ce-NCP. By contrast, under identical conditions, the cascade activity of the co-encapsulated ChOx and HRP in ZIF-8 (ChOx&HRP@ZIF-8) was significantly inhibited, yielding a much lower oxTMB absorbance. Apparently, the substrate inhibition effect was not occurred in ChOx@Ce-NCP, which may be ascribed to the excellent stability of Ce-NCP at high concentration of H_2O_2 (**Fig. S14**). Therefore, the dual functions of Ce-NCP (as enzyme host and artificial enzyme) act synergistically to drive cascade reaction, leading to a highly efficient conversion of Chol. In addition, the successful fabrications of ChOx@Ce-NCP with different molar ratios of ChOx and Ce-NCP also substantially implies that controllable mass ratio of building blocks is able to be achieved in this catalyst system.

The steady-state kinetic experiments were performed to further investigate the catalytic property of ChOx@Ce-NCP. **Fig. S15** shows that Chol oxidation catalyzed by ChOx@Ce-NCP follows typical Michaelis-Menten behavior. With the Lineweaver-Burk plots, the maximum initial velocity (V_{max}) of ChOx@Ce-NCP was calculated to be 4.398×10^{-8} M s^{-1}, which is 2.4-fold higher than the mixture system of free ChOx and Ce-NCP (**Table S2**). This enhancement is along with an increase in turnover number (K_{cat}), demonstrating the higher catalytic activity of ChOx@Ce-NCP. However, the affinity of ChOx@Ce-NCP to substrate (Chol) is slightly lower than the mixture system of free ChOx and Ce-NCP, as reflected by its relatively higher K_m value. Moreover, compared with the mixture system of free ChOx and Ce-NCP, the similar K_{cat}/K_m value of ChOx@Ce-NCP indicates that ChOx is intact without any activity loss during the integration of ChOx with Ce-NCP. This is mainly benefited from the adaptive inculsion property of Ce-NCP, except for the contributions from mild sysnthesis condition and good biocompatibilty of building blocks.

In addition to enhanced catalytic performances, ChOx@Ce-NCP also displays outstanding stability under a wider range of conditions. From **Fig. S16a**, we can see that after treating at 60 ^oC for 60 min, more than 70 % of initial activity was maintained in ChOx@Ce-NCP, whereas the mixture system of free ChOx and Ce-NCP was completely inactive. Similarly, in the presence of urea, a well-known denaturant, a superior activity was also observed in ChOx@Ce-NCP, especially at a high concentration of urea (**Fig. S16b**). The results indicate that the stability of ChOx@Ce-NCP against high temperature and urea has been greatly improved. Since the catalytic activity of Ce-NCP was not affected by high temperature and urea, the enhanced stability of ChOx@Ce-NCP can be attributed to confinement effect of Ce-NCP as a compartment, which reduces the ability of ChOx to change its structural configuration. Next, the biological stability of ChOx@Ce-NCP was examined in the presence of trypsin. As shown in **Fig. S16c**, after exposure to excess trypsin for 24 h, ChOx@Ce-NCP can retain 95 % of initial activity, while almost no activity was measured in the mixture system of free ChOx and Ce-NCP. This suggests that Ce-NCP can protect ChOx from the degradation of trypsin, possibly because of the large size of trypsin that limits its diffusion across Ce-NCP. Moreover, compared with the mixture system of free ChOx and Ce-NCP, ChOx@Ce-NCP has a superior storage stability at room temperature (**Fig. S16d**). By conducting successive reaction batches, it was also found that after 6 cycles, nearly 95 % of initial activity still can be retained in ChOx@Ce-NCP (**Fig. S16e**). This reflects the reusability of ChOx@Ce-NCP, which is benefit from the negligible leakage of ChOx from Ce-NCP (**Fig. S16f**).

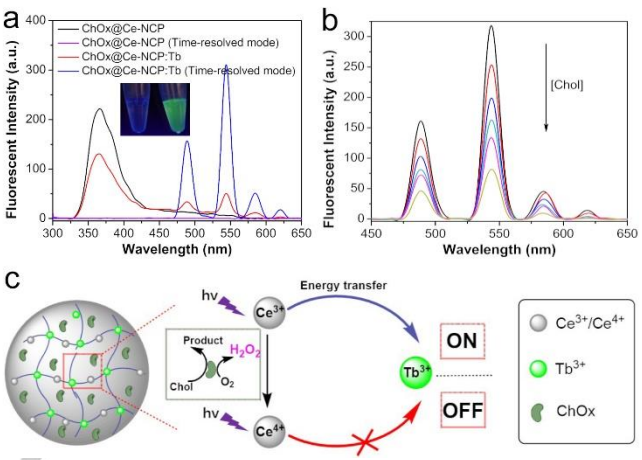

Figure 3. (a) Emission spectra of ChOx@Ce-NCP and ChOx@Ce-NCP:Tb under normal fluorescent model and time-resolved model. Inset is the photography of ChOx@Ce-NCP and ChOx@Ce-NCP:Tb under UV lamp. (b) Emission spectra of ChOx@Ce-NCP:Tb in the presence of Chol. (c) Schematic illustration of the Chol-initiated luminescent switching behavior of ChOx@Ce-NCP:Tb.

Inspired by the fact that Ce^{3+} can transfer its absorbed energy to sensitize Tb^{3+} [14], a luminescent artificial MEC was further fabricated by doping Tb^{3+} in ChOx@Ce-NCP, which generates ChOx@Ce-NCP:Tb. The successful doping of Tb^{3+} was confirmed by the increased Zeta potential (**Fig. S17**) and measured Tb element (**Fig. S18**). Nonetheless, the presence of Tb^{3+} has no influence on the morphology of ChOx@Ce-NCP (**Fig. S19**). Upon the excitation at 290 nm, ChOx@Ce-NCP:Tb emits a green fluorescence and accompanied by the record of five obvious emission peaks (red line in **Fig. 3a**). The peak at 375 nm is consistent to the maximum emission of ChOx@Ce-NCP, while the peaks at 490, 545, 584, and 620 nm correspond to the $^5D_4$ to ^7F_j (j = 3 - 6) electronic transitions of Tb^{3+}. Since no fluorescence was yielded from ChOx@Tb-NCP, which reflects that both ATP and ChOx cannot sensitize Tb^{3+}, the origination of Tb^{3+} emission in ChOx@Ce-NCP:Tb is ascribed to the sensitization effect of Ce^{3+} through an energy transfer process.

Upon the occurrence of energy transfer from Ce^{3+} to Tb^{3+}, a time-resolved fluorescence can be measured in ChOx@Ce-NCP:Tb. **Fig. 3a** shows that under a time-resolved fluorescent mode, ChOx@Ce-NCP:Tb exhibits only Tb^{3+} emission (blue line), but the peak at 365 nm (corresponding to Ce^{3+}) does not be recorded. Meanwhile, it was found that the Tb^{3+} emission is much stronger than that in the case of normal fluorescent mode. This indicates that the background fluorescence of Ce^{3+} in ChOx@Ce-NCP:Tb can be eliminated under time-resolved fluorescent mode, resulting in a high signal-to-noise ratio of Tb^{3+}. **Fig. S20** depicts that to obtain best emission performances, the most suitable ratio of Ce^{3+} to Tb^{3+} in ChOx@Ce-NCP:Tb was at 4:1. On this basis, we discussed the role of ChOx in the emission behaviors of ChOx@Ce-NCP:Tb. From **Fig. S21**, it can be seen that under same conditions, ChOx@Ce-NCP:Tb has a stronger emission intensity and a longer emission lifetime as compared to the mixture system of free ChOx and Ce-NCP:Tb, which is consistent with its higher quantum yields (38.87 % *vs* 19.67 %). This reflects that the encapsulation of ChOx in Ce-NCP:Tb can greatly enhance the emission performances of Tb^{3+}, which may due to the elimination of the quenching effect of water molecule on Tb^{3+} through the coordination reaction of ChOx [15].

Nevertheless, the Tb^{3+} fluorescence in ChOx@Ce-NCP:Tb was obviously quenched in the presence of Chol, as shown in **Fig. 3b**. The XPS spectra of ChOx@Ce-NCP:Tb at different conditions (**Fig. S22**) display that after the addition of Chol, the peaks of Ce^{3+} and Ce^{4+} are both presented in the ChOx@Ce-NCP:Tb. However, in the absence of Chol, only Ce^{3+} peaks were observed. Previously studies have been demonstrated that Tb^{3+} fluorescence can only be sensitized by Ce^{3+} but not Ce^{4+}, and the presence of Ce^{4+} can quench Tb^{3+} fluorescence [14]. Accordingly, the Chol-induced quenching of Tb^{3+} fluorescence is attributed to the oxidation of Ce^{3+} (to form Ce^{4+}) caused by the H_2O_2 as an intermediate in the cascade reaction of ChOx@Ce-NCP.

Encouraged by this finding, we envisioned that the Ce^{3+}/Ce^{4+} redox may be used as a molecular switch to develop a cascade amplified time-resolved fluorescent assay of Chol, as illustrated in **Fig. 3c**. Benefiting from its outstanding cascade activity, the ChOx@Ce-NCP:Tb can detect Chol as low as 42 nM (**Fig. S23**), which is much lower than previously reported methods (**Table S3**). Not only that, compared with previous fluorescent sensors, the ChOx@Ce-NCP:Tb also offers a competitive advantage in eliminating the interferences of nonspecial fluorescence. **Fig. S24** reveals that the presence of ChOx can afford ChOx@Ce-NCP:Tb with specific recognition ability toward Chol over other biological species. The successful determination of Chol in serum sample (**Table S4**) further demonstrates the applicability of ChOx@Ce-NCP:Tb as a luminescent artificial MEC to develop a cascade amplified time-resolved fluorescent assay for Chol sensing.

In summary, a simple and efficient strategy of fabricating artificial MEC has been successfully developed. The integration of ChOx with Ce-NCP was found to endow ChOx@Ce-NCP with higher cascade activity and superior stability than its counterpart, the mixture system of free ChOx and Ce-NCP. More importantly, the distinct advantage of this strategy was also highlighted by its negligible substrate inhibition effect and adjustable mass ratio of building blocks. On this basis, a luminescent artificial MEC was further fabricated by doping Tb^{3+} in ChOx@Ce-NCP and demonstrated to drive a cascade amplified time-resolved fluorescent assay of Chol. Therefore, this work provides a new way to fabricate artificial MEC and which may find applications in biomedical diagnostics and analyses.

Acknowledgements

We gratefully acknowledge the financial support from the Natural Science Foundation of China (21765010 and 21305054).

Keywords: Artificial multi-enzyme complex • Cascade reaction • Catalytic compartment • Nanoscale coordination polymer • Time-resolved fluorescent assay

[1] I. Wheeldon, S. D. Minteer, S. Banta, S. C. Barton, P. Atanassov, M. Sigman, *Nat. Chem.* **2016**, *8*, 299-309.
[2] a) Y. H. P. Zhang, *Biotechnol. Adv.* **2011**, *29*, 715-725; b) E. Ricca, B. Brucher, J. H. Schrittwieser, *Adv. Synth. Catal.* **2011**, *353*, 2239-2262.
[3] a) K. S. Rabe, J. Müller, M. Skoupi, C. M. Niemeyer, *Angew. Chem. Int. Ed.* **2017**, *56*, 13574-13589; b) S. Schoffelen, J. C. M. van Hest, *Soft Matter* **2012**, *8*, 1736-1746; c) J. Shi, Y. Wu, S. Zhang, Y. Tian, D. Yang, Z. Jiang, *Chem. Soc. Rev.* **2018**, *47*, 4295-4313.
[4] a) H. Gustafsson, A. Küchler, K. Holmberg, P. Walde, *J. Mater. Chem. B* **2015**, *3*, 6174-6184; b) L. Hao, S. Jiang, Q. Yuan, G. Li, F. Wang, Z. Zhang, J. Liu, *Nanoscale* **2016**, *8*, 6071-6078; c) X. Wu, J. Ge, C. Yang, M. Hou, Z. Liu, *Chem. Commun.* **2015**, *51*, 13408-13411.
[5] F. Jia, B. Narasimhan, S. Mallapragada, *Biotechnol. Bioeng.* **2014**, *111*, 209-222.
[6] a) H. Tan, S. Guo, N.-D. Dinh, R. Luo, L. Jin, C.-H. Chen, *Nat. Commun.* **2017**, *8*, 663; b) T. Kojima, S. Takayama, *ACS Appl. Mater. Interfaces* **2018**, *10*, 32782-32791.
[7] a) H. Wang, P. Li, D. Yu, Y. Zhang, Z. Wang, C. Liu, H. Qiu, Z. Liu, J. Ren, X. Qu, *Nano Lett.* **2018**, *18*, 3344-3351; b) J. Hou, M. Vázquez-González, M. Fadeev, X. Liu, R. Lavi, I. Willner, *Nano Lett.* **2018**, *18*, 4015-4022; c) H. Wang, C. Liu, Z. Liu, J. Ren, X. Qu, *Small* **2018**, *14*, 1703710; d) Y. Lin, J. Ren, X. Qu, *Acc. Chem. Res.* **2014**, *47*, 1097-1105.
[8] a) J. Wu, S. Li, H. Wei, *Chem. Commun.* **2018**, *54*, 6520-6530; b) N. Kornienko, J. Z. Zhang, K. K. Sakimoto, P. Yang, E. Reisner, *Nat. Nano.* **2018**, *13*, 890-899.
[9] a) W. Kang, J. Liu, J. Wang, Y. Nie, Z. Guo, J. Xia, *Bioconjugate Chem.* **2014**, *25*, 1387-1394; b) A. Grotzky, T. Nauser, H. Erdogan, A. D. Schlüter, P. Walde, *J. Am. Chem. Soc.* **2012**, *134*, 11392-11395.
[10] a) J. Gao, C. Wang, H. Tan, *J. Mater. Chem. B* **2017**, *5*, 7692-7700; b) Y. Fu, P. Li, L. Bu, T. Wang, Q. Xie, J. Chen, S. Yao, *Anal. Chem.* **2011**, *83*, 6511-6517; c) H. Liang, F. Lin, Z. Zhang, B. Liu, S. Jiang, Q. Yuan, J. Liu, *ACS Appl. Mater. Interfaces* **2017**, *9*, 1352-1360; d) H. Liang, B. Liu, Q. Yuan, J. Liu, *ACS Appl. Mater. Interfaces* **2016**, *8*, 15615-15622.
[11] H. Tan, Y. Chen, *Chem. Commun.* **2011**, *47*, 12373-12375.
[12] H. Tan, C. Ma, L. Gao, Q. Li, Y. Song, F. Xu, T. Wang, L. Wang, *Chem. Eur. J.* **2014**, *20*, 16377-16383.
[13] F.-P. Chang, Y. Hung, J.-H. Chang, C.-H. Lin, C.-Y. Mou, *ACS Appl. Mater. Interfaces* **2014**, *6*, 6883-6890.
[14] a) Q. Li, V. W.-W. Yam, *Angew. Chem. Int. Ed.* **2007**, *46*, 3486-3489; b) G. Chen, H. Zhao, F. Rosei, D. Ma, *J. Phys. Chem. C* **2013**, *117*, 10031-10038.
[15] a) F. S. Richardson, *Chem. Rev.* **1982**, *82*, 541-552; b) A. M. Kłonkowski, S. Lis, M. Pietraszkiewicz, Z. Hnatejko, K. Czarnobaj, M. Elbanowski, *Chem. Mater.* **2003**, *15*, 656-663.

10.1002/chem.201902222

WILEY-VCH

Entry for the Table of Contents

Layout 1:

COMMUNICATION

The doping of Tb(III) in ChOx@Ce-NCP leads to a luminescent artificial multi-enzyme complex (ChOx@Ce-NCP:Tb), which combines the merits of cascade catalysis of artificial multi-enzyme complex and unique emission behaviour of Tb(III) and is capable of driving a cascade amplified time-resolved fluorescent assay within a confined space, showing high sensitivity and specificity toward cholesterol.

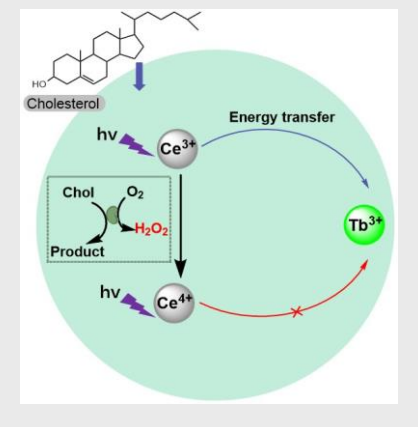

*Jie Gao, Caihong Wang, Jinhong Wang, Hongliang Tan**

Page No. – Page No.

Cascade amplified time-resolved fluorescent assay driven by enzyme-integrated catalytic compartment as an artificial multi-enzyme complex